JOURNAL OF MATERIALS PROCESSING TECHNOLOGY 209 (2009) 1111–1121

journal homepage: www.elsevier.com/locate/jmatprotec

Three-dimensional temperature predictions in machining processes using finite difference method

D. Ulutan, I. Lazoglu, C. Dinc*

Manufacturing & Automation Research Center, Koc University, Rumeli Feneri Yolu, Sariyer, Istanbul 34450, Turkey

ARTICLE INFO

Article history:
Received 9 August 2007
Received in revised form
28 February 2008
Accepted 17 March 2008

Keywords:
3D
Thermal prediction
Finite difference method
Machining
Infrared

ABSTRACT

The purpose of this study is to determine the three-dimensional temperature fields on the chip, tool and workpiece during machining, which is one of the most important characteristic of machining processes; since the fields can affect other properties such as residual stresses and tool wear, and thus tool life and fatigue life of finished parts. The finite difference method (FDM)-based model proposed in this paper offers very rapid and reasonably accurate solutions. Finite difference-based simulation results are validated with infrared thermal measurements which are determined from the machining of AISI 1050 and AISI H13 materials under various cutting conditions.

1. Introduction

Over the past few decades, many academicians studied the characteristics of machining processes, using numerical, analytical and experimental techniques. Prediction and measurement of machining forces, temperatures, tool wear, residual stresses and many other characteristics are performed with substantial care, and many good agreements are found between numerical/analytical solutions and experimental data. Temperature field is one of the most important properties of a machining process; since the field can affect other characteristics such as residual stresses and tool wear.

Prediction of temperature distribution is generally engineered using finite element-based models, which takes long time. Another way used widespread is to employ curve fitting: relating temperature distribution to cutting parameters and tool and workpiece properties by fitting a curve to temperature experiments. However, this method is not fully based on physical phenomena. Therefore, there is a need for rapid and accurate solution to the temperature prediction problem based fully on physical phenomena, which is found by using finite difference-based model proposed in this paper.

Investigation of heat partition in high speed turning of high strength alloy steel.

It is known that the most widespread way to predict cutting temperatures on chip, tool and workpiece, in orthogonal machining, is FEM-based methods. Many studies on the issue are present on simulation of several process outputs such as cutting forces, stresses and temperature fields on chip, tool and workpiece, employing FEM-based models. Özel and Altan (2000) simulated temperatures in high speed flat end milling. Abukshim et al. (2005) investigated high partition in high speed machining. Fang and Fang (2007) analyzed rounded edge tools. Özel (2006) and Filice et al. (2007a) made analyses on friction modeling in machining. Ren et al. (2007) looked at the temperatures in hard turning.

* *Corresponding author*. Tel.: +90 212 338 1587; fax: +90 212 338 1548.
E-mail address: ilazoglu@ku.edu.tr (I. Lazoglu).
0924-0136/$ – see front matter © 2008 Elsevier B.V. All rights reserved.
doi:10.1016/j.jmatprotec.2008.03.020

Grzesik (2006a) used analytical results as input to a FEM-based model to determine temperature distribution on uncoated and three-layer coated tools. Shatla et al. (2001) predicted cutting temperature using FEM and analytical approaches, by determining the flow stress and investigating the effect of edge preparation on cutting forces, stresses and temperatures.

Many researchers also used algorithms like curve fitting to predict temperature fields and parameters leading to temperature fields in machining processes. Umbrello et al. (2007a) did such an analysis to find the heat transfer coefficient, and simulated the transient thermal conditions by a FEM-based method and the artificially modified heat transfer coefficient (Umbrello et al., 2007b). Filice et al. (2007b) tried to predict wear in orthogonal machining using linear and polynomial models using a FE-based temperature prediction method. Yvonnet et al. (2006) offered an inverse procedure to predict the temperatures. Kwon et al. (2001) also used an inverse method to predict the average steady-state rake face temperature fields in cutting processes. They made this prediction by measuring the cooling state of the tool, and inputting it to the spatial and temporal equations of heating of the tool as a boundary condition. Carvalho et al. (2006) also proposed an inverse method to predict cutting temperatures, using a finite volume model to solve the three-dimensional heat diffusion equation.

There are also other analytical/numerical studies to predict the temperature field, average temperature or maximum temperature at the rake face (Grzesik, 2006b; Grzesik and Nieslony, 2004), where an analytical approach was used while using multilayer coated tools in orthogonal turning. Chou and Song (2005) developed an analytical model to predict cutting temperatures on the tool, and investigated the effect of temperature on the wear of the tool. Komanduri and Hou (2000) modeled the heat flux due to shearing in the primary heat zone, and the temperature rise due to this heat flux. They resulted that the maximum temperature rise due to shearing happens at the shearing zone, far from tool–chip contact face.

Finite difference-based models offer considerably less computational time compared to FEM-based models with good accuracy, and more reliable results than curve fitting algorithms, since these methods offer analytical/numerical solutions. Lazoglu and Altintas (2002) created such a two-dimensional finite difference-based model to predict cutting temperatures in continuous (turning) and interrupted machining (milling) based on prediction of cutting forces, and primary and secondary zone heat generation terms. Ulutan et al. (2007) used this method and improved it to predict residual stresses occurring on the workpiece after the tool finishes its way on it. Both studies compared their results with experimental findings and concluded that the numerical solution is in good agreement with measurements. Grzesik and Nieslony (2004) predicted the tool–chip interface temperatures in machining AISI 1050 steel, using an FDM-based model they created, and resulted that the simulations are in good agreement with measurements.

There are also studies to use measurement techniques to improve the results of simulations. Sreejith et al. (2007) monitored the acoustic emission signals during machining, followed by a multiple regression analysis to model the temperature of machining. Experimentations alone can be observed within literature as well, to see the effect of some parameters mostly. Boud (2007) conducted experiments while turning carbon steel bar to see the effect of bar diameter on temperature outcome.

Many researchers contributed in the issue by reviewing the studies. Recently, temperature measurement techniques and comparability of previous test results are reviewed, as well as ongoing research on heat generation and dissipation at the tool–chip contact face during orthogonal machining (Abukshim et al., 2006). Filice et al. (2006) investigated the capability of finite element models developed to predict the temperature field in machining, and compared two temperature measurement methods, namely thermocouple method and thermographic analysis. They also investigated the two-dimensional thermo-mechanical and three-dimensional pure thermal types of numerical solutions. The analytical and experimental methods used to predict and measure temperature during machining are also reviewed (da Silva and Wallbank, 1999).

In this paper, prediction of three-dimensional temperature fields in moving chip, stationary tool and moving workpiece during machining operations is presented; using a finite difference method-based numerical model. The heat transfer from the primary and secondary heat sources (shear plane and friction face) is very crucial due to its brutal results. These results include, but are not limited to rapid wear of the tool, and tensile residual stresses on the surface of end product that cause low fatigue life. First, we study the chip and tool together to create a heat balance due to the friction on the rake face. Then, we investigate the effect of the temperature of chip and tool on the temperature field of the workpiece, taking into account the heat coming from the shear plane. A finite difference-based model is employed to undergo this process, and it can be seen that the results are in good agreement with experimental data presented in the literature. Additionally, the advantage of this method over FEM models is the computational time, which is decreased substantially; and the advantage over curve fitting methods is that the method is fully based on physical explanation.

2. Thermal modeling of chip, tool and workpiece in 3D

2.1. *Heat balance*

Before starting to employ the finite difference method, analytical solution of the problem must be reviewed carefully. Everything concerning the heat balance comes from the first law of thermodynamics, which can be summarized as conservation of energy, or in a more explanatory way: summation of the rate difference that thermal and mechanical energy enter and exit the control volume, and the rate of heat generation, is equal to the rate of energy stored within the control volume. In symbolic terms that explain the heat and mass transfer phenomena

$$\dot{E}_{\text{in}} - \dot{E}_{\text{out}} + \dot{E}_{\text{generated}} = \dot{E}_{\text{stored}} \quad (1)$$

2.1.1. Heat balance equations of chip

Considering this energy balance equation, if we define Q_x, Q_y and Q_z as the heat conduction entering the control volume from x, y and z directions, respectively, and the control volume has dimensions of dx, dy, and dz, then the rates of heat conduction are defined as

$$\begin{aligned}\dot{Q}_x &= -kA\frac{\partial T}{\partial x} = -k\,dy\,dz\frac{\partial T}{\partial x}\\ \dot{Q}_y &= -kA\frac{\partial T}{\partial y} = -k\,dx\,dz\frac{\partial T}{\partial y}\\ \dot{Q}_z &= -kA\frac{\partial T}{\partial z} = -k\,dx\,dy\frac{\partial T}{\partial z}\end{aligned} \tag{2}$$

Here, k is the thermal conductivity of the workpiece, and A is the area of the surface that is exposed to this heat conduction. The heat conduction rates exiting the control volume from x, y, and z directions can be found from Taylor series expansion of the derivative of heat conduction rates and ignoring the higher order terms:

$$\begin{aligned}\dot{Q}_{x+dx} &= \dot{Q}_x + \left(\frac{\partial \dot{Q}_x}{\partial x}\right) dx\\ \dot{Q}_{y+dy} &= \dot{Q}_y + \left(\frac{\partial \dot{Q}_y}{\partial y}\right) dy\\ \dot{Q}_{z+dz} &= \dot{Q}_z + \left(\frac{\partial \dot{Q}_z}{\partial z}\right) dz\end{aligned} \tag{3}$$

These equations involve only the heat conduction terms. Since the study is three-dimensional, and the system can be modeled as stationary with air flowing around, there is heat loss by convection from the system (chip, tool and workpiece) to surrounding air. This heat convection is included in the model as heat flow exiting from the control volume to the surroundings, if the control volume under consideration has contact with surroundings. Therefore, this heat convection rate is directed from the control volume to the surrounding air:

$$\dot{Q}_{z,conv} = hA(T - T_\infty) \tag{4}$$

Here, h is the convection coefficient between the chip and the ambient air flowing around. The temperature of ambient air is considered to be close enough to the room temperature; therefore room temperature boundary conditions are used. This term becomes zero if the control volume is not in contact with air, so special care should be taken while using the boundary conditions in finite difference form.

Since the heat generation in the control volume is equal to the volumetric heat generation rate times the volume of the control volume, and the amount of heat stored within the control volume is related to the density ρ, specific heat capacity C_p, and the rate of change in temperature,

$$\begin{aligned}\dot{E}_{generated} &= \dot{Q}dx\,dy\,dz\\ \dot{E}_{stored} &= \rho C_p\frac{\partial T}{\partial t}dx\,dy\,dz\end{aligned} \tag{5}$$

We can write the heat balance equation in chip as

$$\dot{Q}_x + \dot{Q}_y + \dot{Q}_z - \dot{Q}_{x+dx} - \dot{Q}_{y+dy} - \dot{Q}_{z+dz} - \dot{Q}_{z,conv} + \dot{Q}\,dx\,dy\,dz = \rho C_p\frac{\partial T}{\partial t}dx\,dy\,dz \tag{6}$$

The differences of dimensional heat conduction rates become only a partial derivative of heat, which becomes the second derivative of temperature with the corresponding dimension. If we divide both sides by ($k\,dx\,dy\,dz$), assuming that the heat conduction coefficient and heat convection coefficient are constant both with time and space, and define $\alpha = k/(\rho C_p)$, we can simplify the heat balance equation for chip as

$$\frac{\partial^2 T}{\partial x^2} + \frac{\partial^2 T}{\partial y^2} + \frac{\partial^2 T}{\partial z^2} + \frac{\dot{Q}}{k} - \frac{h(T - T_\infty)}{k\Delta z} = \frac{1}{\alpha}\frac{\partial T}{\partial t} \tag{7}$$

The equation is now in a form that finite difference method can be applied on, with second-order approximations on spatial second derivatives, and first-order approximation on temporal first derivative, which will be converted to a first-order spatial derivative using the moving chip theory.

2.1.2. Heat balance equations of tool

The same equation can be written for the tool employing the heat balance equation in cylindrical coordinates for a control volume of dimensions dr, $r\,d\psi$, dz, and simplifying the corresponding elements and treating the heat conduction coefficient constant with time and space as:

$$\frac{\partial^2 T}{\partial r^2} + \frac{1}{r}\frac{\partial T}{\partial r} + \frac{1}{r^2}\frac{\partial^2 T}{\partial \psi^2} + \frac{\partial^2 T}{\partial z^2} + \frac{\dot{Q}}{k} - \frac{h(T - T_\infty)}{k\Delta z} = \frac{1}{\alpha}\frac{\partial T}{\partial t} \tag{8}$$

2.1.3. Heat balance equations of workpiece

Workpiece is modeled as a rectangular prism, which is the same as chip model. This means that Cartesian coordinates are used to define the heat balance equations, same as 3D chip model:

$$\frac{\partial^2 T}{\partial x^2} + \frac{\partial^2 T}{\partial y^2} + \frac{\partial^2 T}{\partial z^2} + \frac{\dot{Q}}{k} - \frac{h(T - T_\infty)}{k\Delta z} = \frac{1}{\alpha}\frac{\partial T}{\partial t} \tag{9}$$

2.2. Finite difference equations of chip, tool and workpiece

Since it is hard to solve three-dimensional heat balance equations analytically, and it is not even possible most of the times with conventionally used methods, it is important to apply numerical techniques such as finite element method or finite difference method. This part of the study deals with the finite difference equations of chip, tool and workpiece that are used to predict the temperature fields. The difference between the solutions of analytical and numerical solutions is that in numerical solution, the field is subdivided into smaller segments (grids). These elements generally have the same size and dimensions for simplicity. In Fig. 1, a two-dimensional grid is employed on the field and the temperature of the node under consideration is written with respect to the temperatures of the neighboring nodes. These neighboring nodes are

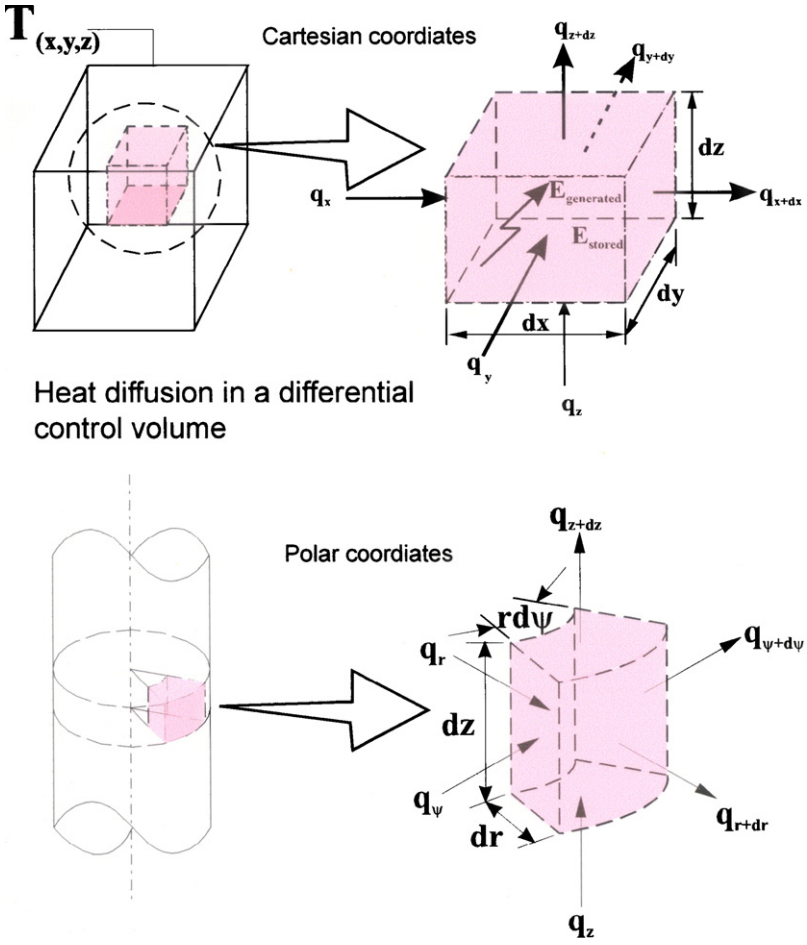

Fig. 1 – Coordinate axes and differential amounts for Cartesian and polar coordinates.

shown in Fig. 2, with a closer look to the specific node that we consider. Likewise, the first and second spatial derivatives of the temperature of the node under consideration can be written by using the temperatures of the same node and its neighboring nodes as:

$$\begin{aligned}
\frac{\partial T}{\partial x} &\cong \frac{T_{x+\Delta x,y,z} - T_{x-\Delta x,y,z}}{2\Delta x}\\
\frac{\partial^2 T}{\partial x^2} &\cong \frac{T_{x+\Delta x,y,z} + T_{x-\Delta x,y,z} - 2T_{x,y,z}}{(\Delta x)^2}\\
\frac{\partial^2 T}{\partial y^2} &\cong \frac{T_{x,y+\Delta y,z} + T_{x,y-\Delta y,z} - 2T_{x,y,z}}{(\Delta y)^2}\\
\frac{\partial^2 T}{\partial z^2} &\cong \frac{T_{x,y,z+\Delta z} + T_{x,y,z-\Delta z} - 2T_{x,y,z}}{(\Delta z)^2}\\
\frac{\partial T}{\partial r} &\cong \frac{T_{r+\Delta r,\psi,z} - T_{r-\Delta r,\psi,z}}{2\Delta r}\\
\frac{\partial^2 T}{\partial r^2} &\cong \frac{T_{r+\Delta r,\psi,z} + T_{r-\Delta r,\psi,z} - 2T_{r,\psi,z}}{(\Delta r)^2}\\
\frac{\partial^2 T}{\partial \psi^2} &\cong \frac{T_{r+\Delta\psi,\psi,z} + T_{r,\psi-\Delta\psi,z} - 2T_{r,\psi,z}}{(\Delta\psi)^2}
\end{aligned} \tag{10}$$

The Cartesian approximations were used for chip and workpiece, while the polar form approximations were used for the tool.

For the chip, Eq. (11) can be found using these approximations. Writing this equation in matrix form with nodal temperatures being the unknown, coefficients of the temperatures constituting the coefficient matrix, and the T^0 coefficients being the RHS of the equation, one can solve the matrix problem using Gaussian elimination (Eq. (12)).

$$\begin{aligned}
&\frac{T_c(x+\Delta x,y,z) + T_c(x-\Delta x,y,z) - 2T_c(x,y,z)}{(\Delta x)^2}\\
&+\frac{T_c(x,y+\Delta y,z) + T_c(x,y-\Delta y,z) - 2T_c(x,y,z)}{(\Delta y)^2}\\
&+\frac{T_c(x,y,z+\Delta z) + T_c(x,y,z-\Delta z) - 2T_c(x,y,z)}{(\Delta z)^2}\\
&-\frac{V_c}{\alpha}\frac{T_c(x+\Delta x,y,z) - T_c(x-\Delta x,y,z)}{2\Delta x}\\
&-\frac{hT_c(x,y,z)}{k\,\Delta z} = \frac{-\dot{Q}}{k} - \frac{hT_\infty}{k\,\Delta z}
\end{aligned} \tag{11}$$

$$[A]\{T_c\} = \{C\} \Rightarrow \{T_c\} = [A]^{-1}\{C\} \tag{12}$$

For the tool, radial, angular and longitudinal (cylindrical) approximations are used, and Eq. (13) is gathered combining

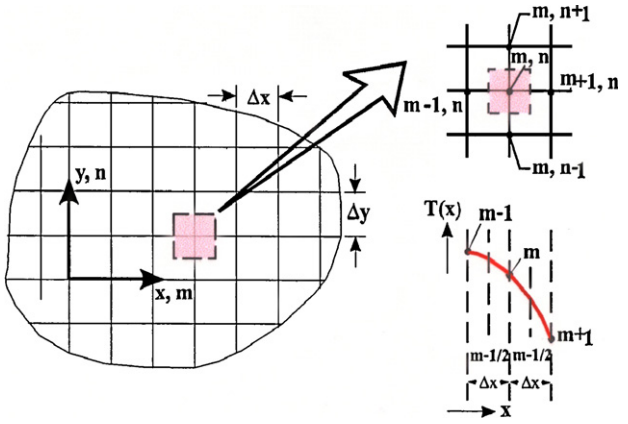

Fig. 2 – Closer look to the specific node under consideration.

these. Again, grouping the nodal temperatures and coefficients at one side, with T^0 coefficients at the other, the matrix problem can be solved (Eq. (14)).

$$\frac{T_t(r+\Delta r,\psi,z)+T_t(r-\Delta r,\psi,z)-2T_t(r,\psi,z)}{(\Delta r)^2} + \frac{T_t(r,\psi+\Delta\psi,z)+T_t(r,\psi-\Delta\psi,z)-2T_t(r,\psi,z)}{r^2(\Delta\psi)^2} + \frac{T_t(r,\psi,z+\Delta z)+T_t(r,\psi,z-\Delta z)-2T_t(r,\psi,z)}{(\Delta z)^2} + \frac{T_t(r+\Delta r,\psi,z)-T_t(r-\Delta r,\psi,z)}{2r\,\Delta r} - \frac{hT_t(r,\psi,z)}{k\,\Delta z} = \frac{-\dot{Q}}{k} - \frac{hT_\infty}{k\,\Delta z} \quad (13)$$

$$[D]\{T_t\} = \{E\} \Rightarrow \{T_t\} = [D]^{-1}\{E\} \quad (14)$$

For the workpiece, heat balance equations in finite difference form are analogous to the equations of chip, with the only difference being T_w instead of T_c. Therefore, Eq. (15) can be achieved by grouping the corresponding terms together.

$$[R]\{T_w\} = \{S\} \Rightarrow \{T_w\} = [R]^{-1}\{S\} \quad (15)$$

Once these equations are employed to solve the analytical problem and the corresponding temperature values are written, the inlet and exit heat conduction terms are handled within the equation. The only thing that remains becomes the heat generation.

2.3. *Heat generation*

There are three main heat generation zones during the machining processes, which are named primary, secondary and tertiary zones. Since we are dealing with orthogonal machining, tertiary zone heat generation is theoretically not observed. Primary zone heat generation due to shearing, and secondary zone heat generation due to friction at the rake face are modeled per unit depth of cut. These heat generation values are found from the force and velocity components along shear and friction dimensions, such as

$$Q_s = F_s V_s = \frac{\tau h V \cos(\alpha_n)}{\sin(\alpha_n)\cos(\phi_n-\alpha_n)}$$
$$Q_f = F_f V_c = \frac{\tau h V \sin(\beta_n)}{\cos(\phi_n+\beta_n-\alpha_n)\sin(\phi_n-\alpha_n)} \quad (16)$$

In these equations, h is the uncut chip thickness, which corresponds to feedrate in turning, τ is the shear flow stress, V is the cutting velocity and α_n, ϕ_n and β_n are the normal rake angle, normal shear angle and normal friction angle, respectively. These values of heat generation are found per unit depth of cut; but multiplying them by depth of cut would give the actual values. Then, by dividing to the amount of nodes along the depth of cut, one can find the amount of heat generated at any node at the heat generation surface.

2.3.1. *Distribution of heat generation in the primary zone*

Heat generated at the shear plane is distributed between chip and workpiece. Since we look at the tool–chip contact first, we modeled this heat generation as a heat source that raises the temperature of the nodes at the shear plane. However, since the specific values of the temperature rise at the nodes is hard to find, the average temperature rise is found according to Oxley's energy partitioning function, and is used as a boundary condition at the nodes on chip that has just started to shear.

$$\Delta T = \frac{Q_s(1-B2)}{\rho C_p h V} \quad (17)$$

where ρ is the density of the workpiece, C_p is the specific heat capacity of the workpiece, h is the uncut chip thickness, V is the cutting velocity, Q_s is the shear plane heat generation per unit depth of cut and B2 is the proportion of shearing heat flux that has entered the workpiece. This value can be found by the following approximations (Lazoglu and Altintas, 2002):

$$B2 = 0.5 - 0.35\log(R_t\tan(\phi_n)) \quad \text{if } 0.004 < R_t\tan(\varphi_n) < 10$$
$$B2 = 0.5 - 0.15\log(R_t\tan(\phi_n)) \quad \text{if } R_t\tan(\varphi_n) > 10 \quad (18)$$

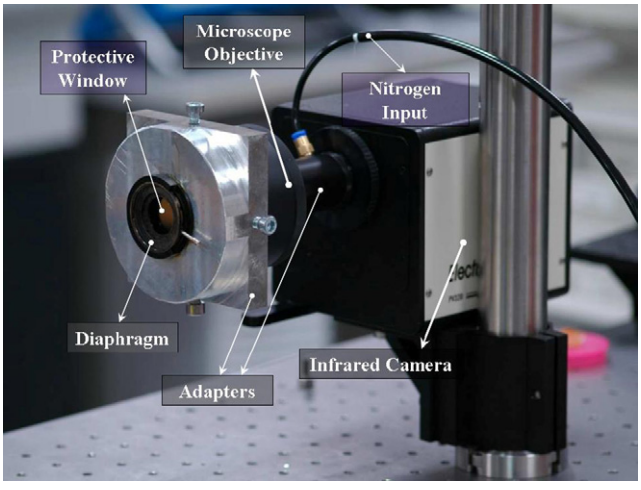

Fig. 3 – The infrared camera system used for temperature measurements.

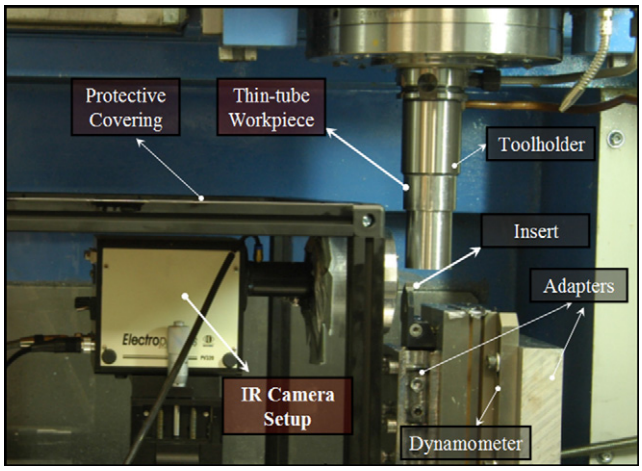

Fig. 4 – The IR camera system as it is in the vertical CNC machine.

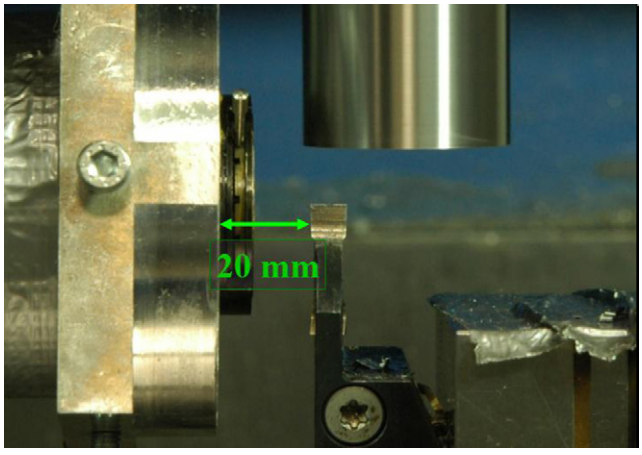

Fig. 5 – The close-up view of the IR system near the tool insert.

Here, φ_n is the normal shear angle and R_t is called the thermal number found by

$$R_t = \frac{\rho C_p h V}{k} \quad (19)$$

2.3.2. Distribution of heat generation in the secondary zone

Heat generation in the secondary zone is more complexly handled than the heat generation in the primary zone. Here, we first assume a portion of heat generated due to friction flows to the tool, and after solving chip and tool temperature fields, we compare the rake face temperatures. Since these nodes on chip and tool are actually the same points on space, the temperature difference between the two must be theoretically zero. However, reaching this zero difference is very hard and time consuming in numerical solutions, if not impossible. This is due to the characteristic of numerical solution methods, the convergence of the element size. Hence, a difference below an acceptable tolerance limit is expected. If the difference is not under the tolerance limits, the portion of heat generation flowing to the tool is updated in such a fashion that this difference might be smaller. Iteratively, this difference is pulled below the tolerance limits and the temperatures of tool and chip rake face nodes are brought close together.

3. Experimental procedure

Temperature field observed on the tool is measured with an infrared camera, and compared to simulations for three-dimensional tool temperature field, concerning the maximum rake face temperature at the tool from an orthogonal point of view. The infrared (IR) camera technique has many advantages to measure temperature in machining processes. These advantages include zero contact between the camera and the heat sources, therefore no effect on temperature distribution, and fast response of the IR camera system. While using other methods such as thermocouples or fiber-optic pyrometer, the measurement device has to be embedded within the tool, which perturbs the heat flow in the tool and changes the results. In addition, fast response of the IR camera lets high cutting speeds to be used in machining experiments, since it becomes possible to capture the transient changes.

The technique has some disadvantages as well, such as the need of knowledge about the exact surface emissivity and chip obstruction. To make the measurements accurate with the IR camera, one needs to know the exact surface emissivity, which changes with surface temperature, roughness and phase of the material, all of them changing during the process. Furthermore, during the process, flowing chip may get between the tool and the camera, which will obstruct the measurements. This disadvantage is handled by repeatedly doing the measurements until getting the best chip-free view.

The IR camera used in the experiments can be seen in Fig. 3. The main part of this system is the IR camera, whose model is Electrophysics PV-320, having an uncooled focal plane array (FPA) detector – which takes advantage of a ferroelectric phase transition in certain dielectric materials – and utilizing an array of pyroelectric elements in that plane, which is a ceramic

Table 1 – Cutting parameters and orthogonal cutting results for all workpiece–tool combinations

Material	Tool rake angle (°)	Cutting speed (m/min)	Feedrate (mm)	Shear angle (°)	Friction angle (°)	Shear flow stress (MPa)
AISI 1050	6	60, 80	0.050, 0.075, 0.100	32.2	41.9	644.9
	18			33.7	42.4	825.0
AISI H13	6	40, 60	0.050, 0.075, 0.100	37.5	36.1	772.2
	18			33.9	43.2	1076.3

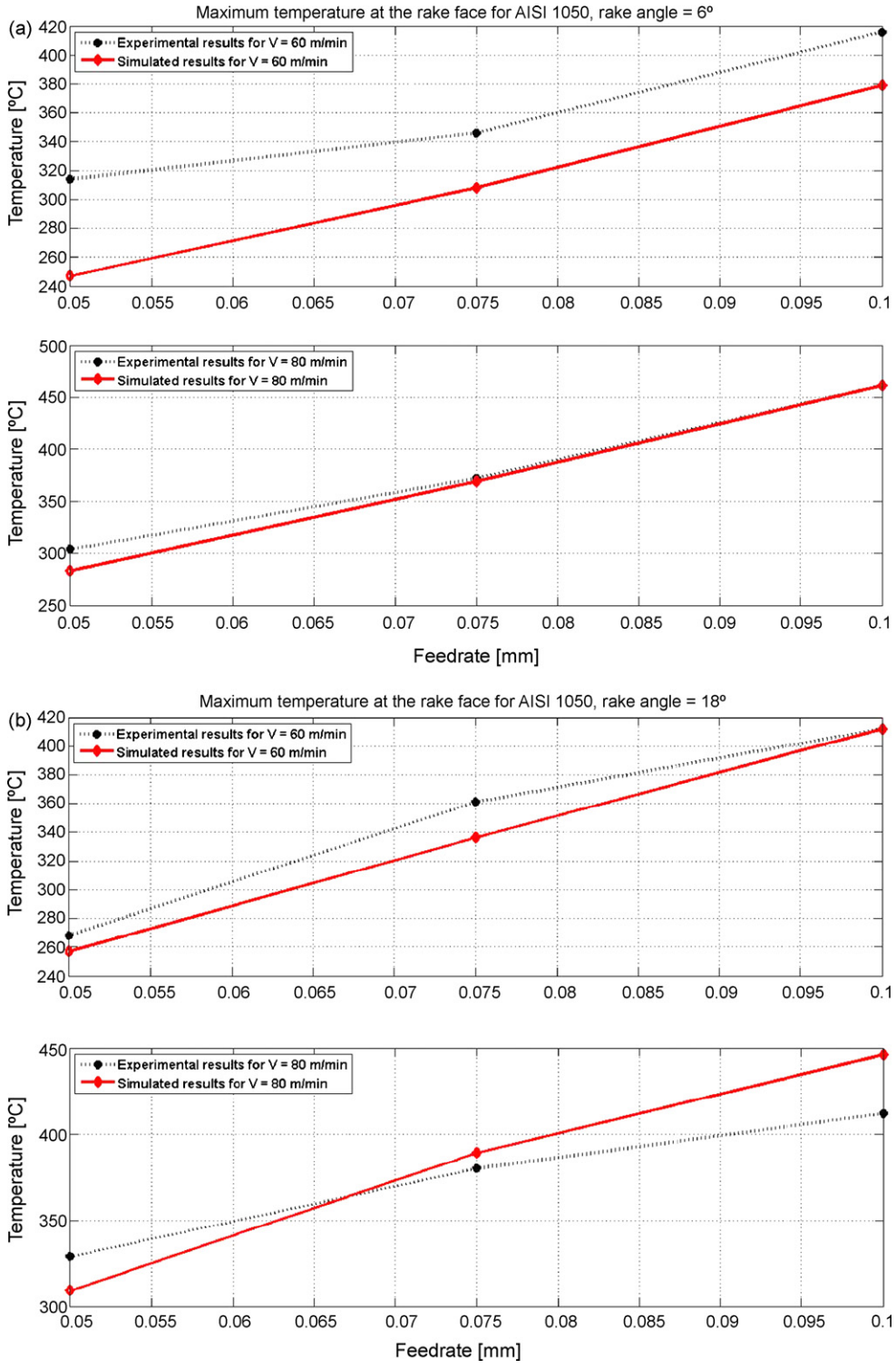

Fig. 6 – Maximum temperature comparison of simulations and experiments for AISI 1050 workpiece material, for (a) tool having 6° of rake angle and (b) tool having 18° of rake angle.

material of barium, strontium and titanium salts. The nominal desired composition of the ceramic is Ba0.66 Sr0.34 TiO3. The IR camera has 320×240 pixels of array size, a target image temperature range between $-18\,^{\circ}C$ and $523\,^{\circ}C$, and a minimum resolvable temperature difference of approximately $0.2\,^{\circ}C$ at $25\,^{\circ}C$. The spectral responsivity of the camera is 7–14 μm, and the camera has 2:1 interlace scanning property. The diaphragm adjusts the IR light intensity that enters into the camera. The nitrogen input is needed in order to overcome the condensation problem due to the humid environment, since this condensation can cause noises in the final captured IR image. The reflective microscope objective images the

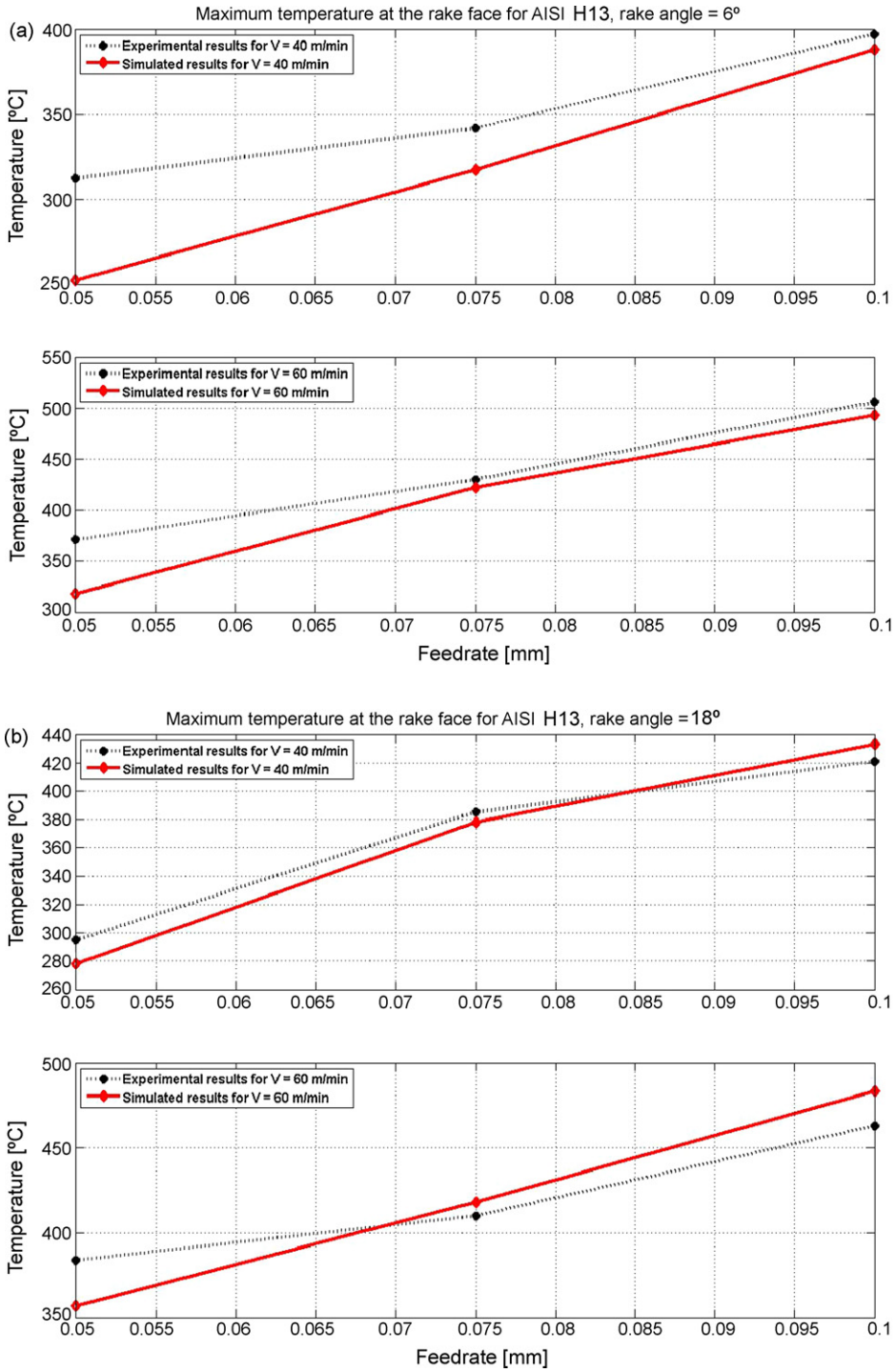

Fig. 7 – Maximum temperature comparison of simulations and experiments for AISI H13 workpiece material, for (a) tool having 6° of rake angle and (b) tool having 18° of rake angle.

area of interest on to the FPA detector. The protective window prevents chips to harm the objective.

Fig. 4 shows the same IR camera system adapted into the Vertical CNC Milling Center, in which the measurements are done. As seen in the figure, during the temperature measurements in the CNC machine, the IR setup is protected with an additional covering in order to isolate the camera and the objective from the chips and any flying particles that are present in the environment of CNC machine. The tool is placed in the workpiece location, since it has to be steady to measure correctly, and the workpiece is placed in the tool location, rotating with the spindle, forming a vertical turning machine. The experiments were done with two different workpiece materials, namely AISI 1050 carbon steel and AISI H13 steel. Cutting inserts were Sandvik, type H13A, which are tungsten carbide inserts without any coating or chip breakers.

Table 2 – Material properties for AISI 1050 and AISI H13

Material	Thermal conductivity (W/mK)	Density (kg/m^3)	Specific heat capacity (J/kg K)	Thermal expansion coefficient (10^{-6}/K)	Elastic modulus (GPa)
AISI 1050	51.9	7870	486	7.8	205
AISI H13	28.6	7760	523	10.4	209

Half of the tests were done with fresh tools having a rake angle of 6°, with edge radius of approximately 15 μm, and the other half with fresh tools having a rake angle of 18°, with edge radius of approximately 20 μm. The force measurement system included a three-component Kistler dynamometer, a Kistler charge amplifier, and a National Instruments I/O box, with data acquisition carried out by MALDAQ (Manufacturing Automation Laboratory Data Acquisition) software, a module of CutPro.

Fig. 5 shows a close-up view of the experimental setup, where the insert (tool) and the workpiece can be seen with a closer view than in Fig. 4. Here, the distance between the aluminum adapter in front of the microscope and the tool rake face is approximately 20 mm. It can be resulted from this fact that making these experiments very close to the cutting edge of the tool in the CNC machine is very difficult, and this distance also explains the need for the additional protective covering.

Finally, the video output from the IR camera is processed by differentiating, noise filtering, and coloring, to get the final results.

4. Simulations and validations

The aforementioned finite difference-based model is applied for different machining conditions and compared with experimental results. Since heat convection is included, chip, tool and workpiece temperatures were observed to be at maximum at the middle part of the system. The effect of the heat convec-

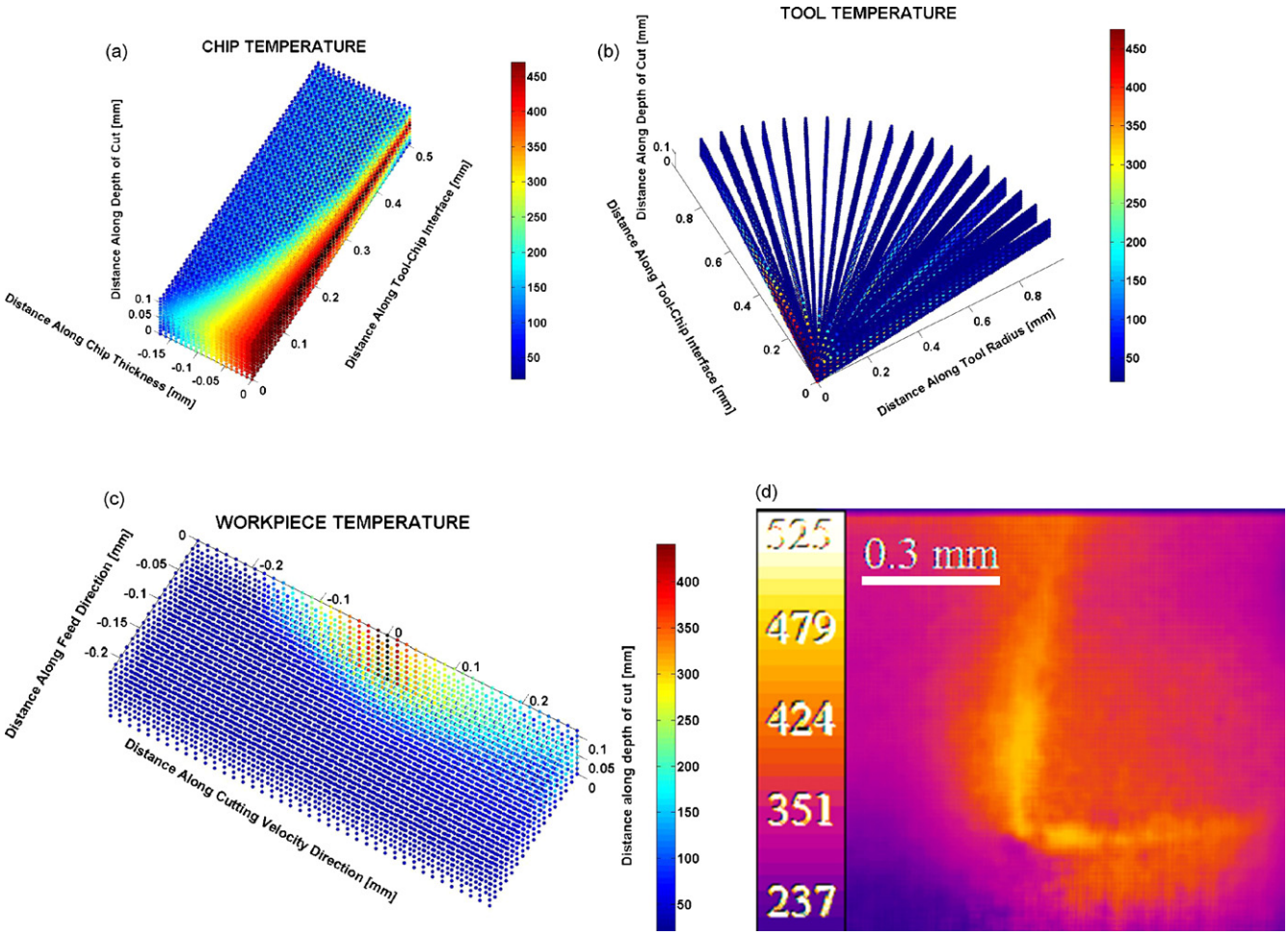

Fig. 8 – Simulated and measured results of temperature for AISI 1050 workpiece material and tool having 6° of rake angle, $V = 80$ m/min and $h = 0.1$ mm. (a) Simulated chip temperature field. (b) Simulated tool temperature field. (c) Simulated workpiece temperature field. (d) Measured tool temperature field.

tion is at minimum due to the fact that it is the furthest piece from both sides that are subjected to heat convection. However, temperatures close to the edge at both sides drop closer to room temperature, as expected. The cutting conditions for Figs. 6 and 7 can be found from Table 1, along with orthogonal cutting parameters for every workpiece–tool combination.

Heat convection coefficient can be determined using air at room temperature flowing at cutting speed as surroundings, stationary system, and approximation of the system to a flat plane. However, cutting velocity component at chip flow direction is used for the heat convection coefficient of chip–air interface. Eq. (20) is used to calculate the heat convection coefficient.

$$Nu_L = 0.664\, Re^{1/2}\, Pr^{1/3} = \frac{hL}{k} \tag{20}$$

Here, Re is the Reynolds number and Pr is the Prandtl number concerning tool, workpiece and machining properties. L is the length of contact between air and the system, and k is the thermal conductivity of the tool–workpiece. Nu_L is the Nusselt number of the process.

5. Results

Orthogonal cutting and temperature measurement tests are done for conditions given in Table 1. Simulations are also made for the cutting conditions given in Table 1. Orthogonal cutting results for shear angle, friction angle and shear flow stress for every tool–workpiece combination is given in Table 1, as well. Table 2 shows the related material properties for both of the workpiece materials. Fig. 8 shows a sample simulation and measurement for AISI 1050 workpiece material, 6° of rake angle for the tool and cutting speed of 80 m/min, feedrate of 0.1 mm. Figs. 6 and 7 show the maximum rake face temperature comparisons between simulations and measurements for all the tool–workpiece combinations and cutting parameters. It can be resulted that the simulations are in acceptable agreement with measurements, although underpredicting 20–60 °C for low feedrate values. This is mostly due to the fact that for low temperatures (temperatures closer to room temperature), thermal conductivity and density of materials change, which will affect Reynolds number of the process and thus heat convection coefficient. Thermal conductivity change will also effect the calculations of chip–tool interface heat generation terms, and perturb the simulation results. Since the calculations for thermal conductivity and density of the materials are done for maximum temperatures that are present, approximately 400 °C, the simulations are most valid for temperature results close to this value.

6. Conclusions

In this paper, three-dimensional finite difference-based model to predict temperature in machining processes is presented. Heat balance equations in three-dimensions are solved analytically for chip, tool and workpiece including the heat convection effect that is excluded in two-dimensional analysis. The main advantage of this method compared to the finite element-based models presented in literature is the computational time, decreasing from hours to minutes, without compromising from accuracy so much. This 3D thermal modeling is critical and input to the residual stress prediction, which is one of the other important current topics in the machining research community.

Acknowledgement

The authors would like to acknowledge the Scientific and Technical Research Council of Turkey (TUBITAK) for its support on the project (TUBITAK Project No: 104M287).

REFERENCES

Abukshim, N.A., Mativenga, P.T., Sheikh, M.A., 2005. Investigation of heat partition in high speed turning of high strength alloy steel. Int. J. Mach. Tools Manuf. 45, 1687–1695.

Abukshim, N.A., Mativenga, P.T., Sheikh, M.A., 2006. Heat generation and temperature prediction in metal cutting: a review and implications for high speed machining. Int. J. Mach. Tools Manuf. 46, 782–800.

Boud, F., 2007. Bar diameter as an influencing factor on temperature in turning. Int. J. Mach. Tools Manuf. 47, 223–228.

Carvalho, S.R., e Silva, S.M.M.L., Machado, A.R., Guimarães, G., 2006. Temperature determination at the chip–tool interface using an inverse thermal model considering the tool and tool holder. J Mater. Process. Technol. 179, 97–104.

Chou, Y.K., Song, H., 2005. Thermal modeling for white layer predictions in finish hard turning. Int. J. Mach. Tools Manuf. 45, 481–495.

Fang, N., Fang, C., 2007. Theoretical and experimental investigations of finish machining with a rounded edge tool. J. Mater. Process. Technol. 191, 331–334.

Filice, L., Micari, F., Rizzuti, S., Umbrello, D., 2007a. A critical analysis on the friction modeling in orthogonal machining. Int. J. Mach. Tools Manuf. 47, 709–714.

Filice, L., Micari, F., Settineri, L., Umbrello, D., 2007b. Wear modeling in mild steel orthogonal cutting when using uncoated carbide tools. Wear 262, 545–554.

Filice, L., Umbrello, D., Beccari, S., Micari, F., 2006. On the FE codes capability for tool temperature calculation in machining processes. J. Mater. Process. Technol. 174, 286–292.

Grzesik, W., 2006a. Determination of temperature distribution in the cutting zone using hybrid analytical-FEM technique. Int. J. Mach. Tools Manuf. 46, 651–658.

Grzesik, W., 2006b. Composite layer-based analytical models for tool–chip interface temperatures in machining medium carbon steels with multi-layer coated cutting tools. J. Mater. Process. Technol. 176, 102–110.

Grzesik, W., Nieslony, P., 2004. Physics based modeling of interface temperatures in machining with multiplayer coated tools at moderate cutting speeds. Int. J. Mach. Tools Manuf. 44, 889–901.

Komanduri, R., Hou, Z.B., 2000. Thermal modeling of the metal cutting process. Part I. Temperature rise distribution due to shear plane heat source. Int. J. Mech. Sci. 42, 1715–1752.

Kwon, P., Schiemann, T., Kountanya, R., 2001. An inverse estimation scheme to measure steady-state tool–chip interface temperatures using an infrared camera. Int. J. Mach. Tools Manuf. 41, 1015–1030.

Lazoglu, I., Altintas, Y., 2002. Prediction of tool and chip temperature in continuous and interrupted machining. Int. J. Mach. Tools Manuf. 42, 1011–1022.

Özel, T., Altan, T., 2000. Process simulation using finite element method—prediction of cutting forces, tool stresses and temperatures in high-speed flat end milling. Int. J. Mach. Tools Manuf. 40, 713–738.

Özel, T., 2006. The influence of friction models on finite element simulations of machining. Int. J. Mach. Tools Manuf. 46, 518–530.

Ren, X.J., Yang, Q.X., James, R.D., Wang, L., 2007. Cutting temperatures in hard turning chromium hardfacings with PCBN tooling. J. Mater. Process. Technol. 147, 38–44.

Shatla, M., Kerk, C., Altan, T., 2001. Process modeling in machining. Part II: Validation and applications of the determined flow stress data. Int. J. Mach. Tools Manuf. 41, 1659–1680.

da Silva, M.B., Wallbank, J., 1999. Cutting temperature: prediction and measurement methods—a review. J. Mater. Process. Technol. 88, 195–202.

Sreejith, P.S., Krishnamurthy, R., Malhorta, S.K., 2007. Effect of specific cutting pressure and temperature during machining of carbon/phenolic ablative composite using PCBN tools. J. Mater. Process. Technol. 183, 88–95.

Ulutan, D., Alaca, B.E., Lazoglu, I., 2007. Analyical modeling of residual stresses in machining. J. Mater. Process. Technol. 183, 77–87.

Umbrello, D., Filice, L., Rizzuti, S., Micari, F., 2007a. On the evaluation of the global heat transfer coefficient in cutting. Int. J. Mach. Tools Manuf. 47, 1738–1743.

Umbrello, D., Filice, L., Rizzuti, S., Micari, F., Settineri, L., 2007b. On the effectiveness of finite element simulation of orthogonal cutting with particular reference to temperature prediction. J. Mater. Process. Technol. 189, 284–291.

Yvonnet, J., Umbrello, D., Chinesta, F., Micari, F., 2006. A simple inverse procedure to determine heat flux on the tool in orthogonal cutting. Int. J. Mach. Tools Manuf. 46, 820–827.